
First Comprehensive Characterization and Ultrasound-Assisted Extraction Optimization of an Unexplored Amazonian Berry (*Chondrodendron tomentosum*): A Novel Source of Anthocyanins and Phenolic Compounds

Disbexy Huaman-Huaman , [Segundo G. Chavez](#) , Laydy Mena-Chacon , [Hans Minchán-Velayarce](#) * , [Ralph Rivera-Botonares](#) *

Posted Date: 5 December 2025

doi: 10.20944/preprints202512.0350.v1

Keywords: response surface methodology; ripening; cyanidin-3-glucoside; underutilized crops; Menispermaceae



Preprints.org is a free multidisciplinary platform providing preprint service that is dedicated to making early versions of research outputs permanently available and citable. Preprints posted at Preprints.org appear in Web of Science, Crossref, Google Scholar, Scilit, Europe PMC.

Copyright: This open access article is published under a [Creative Commons CC BY 4.0 license](#), which permit the free download, distribution, and reuse, provided that the author and preprint are cited in any reuse.

Disclaimer/Publisher's Note: The statements, opinions, and data contained in all publications are solely those of the individual author(s) and contributor(s) and not of MDPI and/or the editor(s). MDPI and/or the editor(s) disclaim responsibility for any injury to people or property resulting from any ideas, methods, instructions, or products referred to in the content.

Article

First Comprehensive Characterization and Ultrasound-Assisted Extraction Optimization of an Unexplored Amazonian Berry (*Chondrodendron tomentosum*): A Novel Source of Anthocyanins and Phenolic Compounds

Disbexy Huaman-Huaman ¹, Segundo G. Chavez ^{1,2}, Laydy Mena-Chacon ², Hans Minchán-Velayarce ^{1,*} and Ralph Rivera-Botonares ^{1,*}

¹ Grupo de Investigación en Compuestos Bioactivos a partir de Matrices Alimentarias y Biológicas - COMBALBI. Universidad Nacional de Jaén, Jaén 06801, Perú

² Instituto de Investigación para el Desarrollo Sustentable de Ceja de Selva (INDES-CES), Universidad Nacional Toribio Rodríguez de Mendoza de Amazonas, Chachapoyas 01001, Perú

* Correspondence: hans.minchan@unj.edu.pe, ralph_rivera@unj.edu.pe; Tel.: +51 941 941 957

Abstract

This is the first scientific report on the fruit characteristics of *Chondrodendron tomentosum* Ruiz & Pav. (Menispermaceae). Biometric and physicochemical parameters were characterized across three fruit ripening stages (green, turning, ripe). Additionally, proximate composition was determined in ripe fruits, and methanol concentration (25–75%), ultrasonic amplitude (30–70%), and time (1–15 min) were optimized using response surface methodology with a Box-Behnken design. During ripening, weight increased by +47.7% (3.89 to 5.74 g; $p < 0.0001$), TSS by +26.1% (7.00 to 8.83 °Brix), pH decreased by 32.0% (6.28 to 4.27), and acidity increased by 276% (0.25 to 0.94%). The quadratic models demonstrated high predictive accuracy ($R^2 > 96.5\%$; $p < 0.004$). Optimal conditions (57% methanol, 70% amplitude, and 15 min) maximized total anthocyanin content (120.71 ± 1.89 mg cyanidin-3-glucoside/L), total phenols (672.46 ± 5.84 mg GAE/100 g), and antioxidant capacity (5857.55 ± 60.20 μ mol Trolox/100 g) in ripe fruits. Anthocyanins were undetectable in green fruits, reaching 46.01 mg C3G/L in turning fruits and 120.71 mg/L in ripe fruits (162% higher than turning fruits). Principal component analysis (90.6% variance) revealed synchronized co-accumulation of anthocyanins and phenols, enhanced by vacuolar acidification. These results position ripe *C. tomentosum* fruits as a raw material for natural colorants, nutraceuticals, and functional foods.

Keywords: response surface methodology; ripening; cyanidin-3-glucoside; underutilized crops; Menispermaceae

1. Introduction

Chondrodendron tomentosum Ruiz & Pav. (Menispermaceae), locally known in northeastern Perú as "uva de montaña" (mountain grape), is an Amazonian woody liana that produces dark purple fleshy drupes arranged in infructescences of 3–6 units [1,2]. The fruits, traditionally consumed in Andean-Amazonian communities, have a sweet-tart flavor and ripen between July and September in montane forests at 1500–2000 m a.s.l. [3]. Despite its traditional use, the phytochemical composition of *C. tomentosum* fruits remains uncharacterized in scientific literature, classifying it as an understudied and underexploited wild species.

Wild Amazonian and Andean berries constitute rich sources of phenolic compounds, anthocyanins, organic acids, and vitamins, with recognized antioxidant, anti-inflammatory, and anticancer properties [4–7]. These secondary metabolites confer nutraceutical value and position wild

species as candidates for functional food development [8]. Additionally, their resistance to adverse climatic conditions and natural immunity to pathogens represent significant agronomic advantages for sustainable production systems [9].

C. tomentosum remains absent from indexed scientific literature: as of November 2025, no studies on fruit composition, bioactive compounds, or extraction methodologies have been reported in databases such as Scopus or Web of Science. This absence in scientific literature simultaneously represents a conservation risk and an unexplored opportunity for functional food development from underutilized tropical biodiversity.

Ultrasound-assisted extraction (UAE) is gaining in importance as a green technology for extracting bioactive compounds from plant matrices by enhancing extraction time, yield, and selectivity over traditional techniques [10,11]. The acoustic cavitation of the ultrasonic probe system, breaking down cell walls, increases mass transfer and reduces thermal degradation of labile metabolites [12,13]. Various berries have shown promising efficiency in collecting anthocyanins and total phenols: *Prunus spinose* [14], *Aronia melanocarpa* [15], *Myrciaria cauliflora* [16], *Myrtus communis* [17], *Morus nigra* [18].

The goal of this analysis was to analyze the biometric and physicochemical properties of *C. tomentosum* at 3 maturity stages (green, turning, and ripe) as well as to assess them along with the proximate characterization of ripe fruits. Ultrasound-assisted extraction (UAE) of phenolic compounds, anthocyanins, and antioxidant capacity from ripe fruits was optimized through Box-Behnken design, evaluating the effect of methanol concentration (25–75%), ultrasonic amplitude (30–70%), and extraction time (1–15 min). Once optimized, the optimal UAE conditions were validated and applied on green and turning stages to evaluate the variation of bioactive compounds during ripening. This study constitutes the first comprehensive scientific report addressing the biometric, physicochemical, proximate, and phytochemical characterization of this species, together with the optimization of green extraction technologies for bioactive compound recovery.

2. Materials and Methods

2.1. Plant Material

Wild fruits of *C. tomentosum* Ruiz & Pav. were collected at green (0), turning (1), and ripe (2) stages (Figure 1) in a montane forest in the village of Villa Rica, San José de Lourdes district, San Ignacio province, Cajamarca, Perú (-5.059457° , -78.892105° ; 1626 m a.s.l.) during July–August 2025. Only healthy fruits without mechanical damage, bruise, or signs of insect or pathogen attack were selected. Taxonomic identification was verified, and the reference specimen (Botanical Determination Certificate No. 05-2024) was deposited in the Isidoro Sánchez Vega Herbarium (ISV), Universidad Nacional de Jaén, Perú. Samples were transported under refrigeration ($4 \pm 1^{\circ}\text{C}$) to the Nutrition and Toxicology Laboratory of the Instituto de Investigación Tecnológico Agroindustrial (IITA), Universidad Nacional del Santa, Chimbote, Perú, for immediate conditioning and processing.

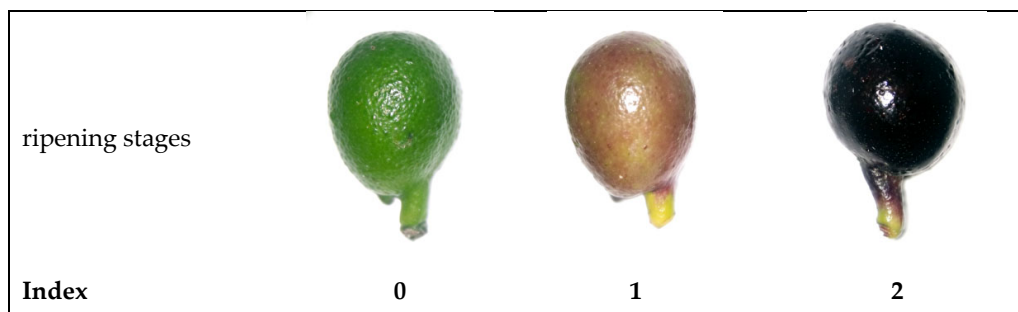


Figure 1. Mountain grape fruits at different ripening stages.

2.2. Chemical Reagents

Folin-Ciocalteu reagent, 2,2-diphenyl-1-picrylhydrazyl (DPPH), (\pm)-6-hydroxy-2,5,7,8-tetramethylchromane-2-carboxylic acid (Trolox), HPLC-grade methanol, potassium chloride, sodium acetate trihydrate, hydrochloric acid (37%), and glacial acetic acid were supplied by Sigma-Aldrich (St. Louis, MO, USA). Anhydrous sodium carbonate was purchased from J.T. Baker (Phillipsburg, NJ, USA), and gallic acid from Merck KGaA (Darmstadt, Germany). Sodium hydroxide and phenolphthalein indicator were of analytical grade.

2.3. Classification of Maturity Stages and Sample Preparation

Fruits were washed with abundant running water, disinfected with sodium hypochlorite solution (80 mg/L) for 2 min, and rinsed with distilled water. Classification by maturity stage was established through a visual colorimetric scale adapted from the maturity index (MI) of olives *Olea europaea* L. [19], defining three categories according to epicarp pigmentation: green (index 0) - uniform green epidermis without pigmentation; turning (index 1) - epidermis with 25–75% purple-reddish pigmentation; ripe (index 2) - uniform dark purple epidermis with >95% pigmented surface (Figure 1).

2.4. Morphological Characterization

Visual observations were performed to describe the *C. tomentosum* plant, as well as the shape, color, and texture of the fruit and seed at three ripening stages [20,21].

2.5. Biometric Characterization

Fifty fruits per maturity stage were evaluated ($n = 50$). The recorded variables were: fresh weight (g), polar diameter (cm), and equatorial diameter (cm). Fresh weight was determined on a precision balance (Precisa, LX-4200C, Switzerland). Diameters were measured with a stainless steel vernier caliper (Pretul, escolar, Mexico) [22]. Polar diameter corresponded to the longitudinal peduncle-style axis; equatorial diameter was measured perpendicularly at the widest zone of the fruit.

2.6. Physicochemical Characteristics

Fruits from each maturity stage were homogenized in a mortar to obtain purée. Vitamin C content was determined by titration using the AOAC 967.21 (2019) [23] method. pH (AOAC 981.12), total soluble solids (AOAC 932.12), and titratable acidity (AOAC 942.15) were developed following standard AOAC methods (2023) [24]. pH was measured with a benchtop pH meter (Hanna, HI2211, Romania) previously calibrated with pH 4.0 and 7.0 buffer solutions. A manual refractometer (Wmeters, REF108, China) was used to estimate total soluble solids (TSS), and values were expressed in °Brix at 20 °C. Titratable acidity (TA) was determined by titrating the sample with an acid-base solution with 0.1 N NaOH to pH 8.8, and results were expressed as percentage of citric acid. The maturity index (MI) was calculated as the TSS/TA ratio [25].

2.7. Proximate Composition

Proximate characterization was performed only on ripe fruits ($n = 3$). Moisture was quantified by gravimetry after drying samples in an oven (POL-EKO/SLW 240, Poland) following the AOAC 945.15 (2023) [24] method. Ash was determined by incineration in a muffle furnace (Protherm Furnaces, PLF 110/6, France) at 550 °C using AOAC 223.03 (2023) [24]. Crude protein was estimated using a Kjeldahl apparatus (Labconco, 6030001, USA) following AOAC 954.01 (2019) [26] with 6.25 as the nitrogen conversion factor. Crude fiber was determined by acid-base hydrolysis following NTP 205.003 (2011) [27], and crude fat by Soxhlet extraction (Marconi, MA-491, Brazil) with petroleum ether as solvent using AOAC 930.09 (2019) [28]. Carbohydrate content was estimated by difference according to the AOAC 986.25 (2023) [24] method using Equation 1.

$$\text{Carbohidratos (\%)} = 100 - (\text{humedad} + \text{proteína} + \text{grasa} + \text{fibra} + \text{cenizas}) \quad \text{Equation 1}$$

2.8. Ultrasound-Assisted Extraction (UAE)

The UAE protocol was adapted from Christou et al. [29] and Razola et al. [30]. Seeds were manually removed, and the pericarp (pulp and peel) was homogenized in a mortar. 1.00 g of sample was weighed into a 50 mL beaker, adding methanolic solution at a 1:30 (w/v) ratio. Extraction was performed using a USCG 1800 ultrasonic homogenizer (Infitek, China) equipped with a titanium sonotrode (\varnothing 18 mm, frequency 24 kHz, nominal power 2500 W). The probe was immersed to approximately 50% of the volume without contact with the vessel walls, operating in continuous mode. Methanol (% v/v), amplitude (%), and time (min) conditions varied according to the Box-Behnken design. Subsequently, extracts were centrifuged (Sigma 4-16KS, Osterode, Germany) at 4200 rpm, 4 °C for 20 min. Supernatants were filtered (Whatman No. 42 paper), protected from light in aluminum foil-wrapped Falcon tubes, and stored at -20 °C until respective analyses.

2.9. Quantification of Total Phenols

Total phenols were determined by the Folin-Ciocalteu spectrophotometric method [31] with modifications. A calibration curve was prepared with gallic acid (0–300 $\mu\text{g/mL}$ in 50% methanol). In amber microtubes, 80 μL of extract was mixed with 160 μL of Folin-Ciocalteu reagent (10% v/v), incubating for 5 min in darkness. 640 μL of Na_2CO_3 (7.5% w/v) was added, and the mixture was incubated for 60 min in darkness at room temperature. Absorbance was measured at 765 nm in a microplate reader (Model Synergy H1, USA). Results were expressed as mg gallic acid equivalents (GAE)/100 g fresh weight basis.

2.10. Quantification of Monomeric Anthocyanins

Total anthocyanins were quantified by the pH differential method [32]. Buffer solutions were prepared: potassium chloride (pH 1.0, 0.025 M) adjusted with concentrated HCl and sodium acetate (pH 4.5, 0.4 M) adjusted with glacial acetic acid. 500 μL of extract was mixed with 500 μL of each buffer independently, homogenizing in a vortex (Model MS 3 digital, Germany). Absorbances were measured at 510 nm and 700 nm in the microplate reader. Monomeric anthocyanin concentration was calculated using Equation 2 and Equation 3:

$$A = (A_{510} - A_{700nm})_{\text{pH}1.0} - (A_{510} - A_{700nm})_{\text{pH}4.5} \dots \text{Equation 2}$$

$$\text{Total Anthocyanins} \left(\frac{\text{mg}}{\text{L}} \right) = \frac{A \times \text{PM} \times \text{FD} \times 1000}{(\epsilon \times l)} \dots \text{Equation 3}$$

Where A is the sample absorbance, MW = 449.2 g/mol (cyanidin-3-glucoside), DF = dilution factor, ϵ = 26900 $\text{L} \cdot \text{mol}^{-1} \cdot \text{cm}^{-1}$, and l = path length in cm. Results were expressed as mg cyanidin-3-glucoside equivalents (C3G)/L.

2.11. Antioxidant Capacity by DPPH

Antioxidant activity was evaluated by the DPPH method [33]. A Trolox stock solution (1 mM) was prepared by dissolving 0.0125 g in 50 mL of methanol. A calibration curve was constructed with Trolox (5–500 μM). A methanolic DPPH solution (1 mM) was prepared, adjusting absorbance to 0.800 ± 0.020 at 515 nm with methanol. In a 96-well microplate, 10 μL of diluted extract (1:5) was mixed with 190 μL of DPPH solution (final volume 200 μL). The mixture was incubated for 30 min in darkness at room temperature, and absorbance was measured at 515 nm in a microplate reader (Model Synergy H1, USA). Results were expressed as μmol Trolox equivalents (TE)/100 g fresh weight basis.

2.12. Experimental Design and Statistical Analysis

RSM using a three-factor Box-Behnken design (15 experimental runs) was applied to optimize UAE. Independent variables were: methanol concentration (A: 25, 50, 75%, v/v), ultrasonic amplitude

(B: 30, 50, 70%), and extraction time (C: 1, 8, 15 min). Response variables were: anthocyanins (mg C3G/L), total phenols (mg GAE/100 g), and antioxidant capacity ($\mu\text{mol TE}/100 \text{ g}$). Data were fitted by least squares to a quadratic polynomial model in coded variables (Equation 4):

$$y = \beta_0 + \beta_A A + \beta_B B + \beta_C C + \beta_{AA} A^2 + \beta_{BB} B^2 + \beta_{CC} C^2 + \beta_{AB} AB + \beta_{AC} AC + \beta_{BC} BC \dots \text{Equation 4}$$

Where y is the predicted response, A , B y C are coded independent variables, β_0 is the intercept, β_A , β_B y β_C are linear coefficients, β_{AA} , β_{BB} y β_{CC} are quadratic coefficients, and β_{AB} , β_{AC} y β_{BC} are interaction coefficients. Optimal conditions were determined using Derringer-Suich's desirability function, simultaneously maximizing the three responses. Analyses were performed using Statgraphics Centurion software (version XVII, USA).

Biometric and physicochemical data were analyzed by one-way ANOVA and Tukey's multiple comparison test ($\alpha = 0.05$) using Minitab software (version 14, USA).

Multivariate exploration was performed through principal component analysis (PCA) on a standardized data matrix (mean-centered, scaled to unit variance) comprising vitamin C, TSS, pH, TA, MI, anthocyanins, total phenols, and antioxidant capacity. A z-score heatmap was generated with annotation by maturity stage. Analyses were executed in R software (version 4.x, USA) with *factoextra* and *ggplot2* packages.

3. Results and Discussion

3.1. Morphological, Biometric, and Physicochemical Characterization During Ripening

3.1.1. Plant and Fruit Morphology

C. tomentosum is a climbing woody liana characterized by large cordate leaves and small whitish-green flowers arranged in axillary inflorescences [1,2] (Figure 2A). The fruits are fleshy ovoid drupes of dark purple color, grouped in clusters of 3-6 units, with scarce mesocarp and sweet-tart flavor [3] (Figure 2B). Each drupe contains a single lunate seed with hard testa, characteristic of Menispermaceae (Figure 2C).

The ontogenic transition from green to ripe involved pronounced changes in epicarp pigmentation and mesocarp firmness (Table 1). The epicarp evolved from intense green and rough (green) to smooth yellowish-red (turning) and glossy blackish-violet (maduro), reflecting chlorophyll degradation and anthocyanin synthesis via the phenylpropanoid pathway [34,35]. The mesocarp transitioned from pale green and firm (green) to semi-soft red (turning) and juicy garnet (ripe), indicating pectin hydrolysis and accumulation of soluble sugars and organic acids [35,36]. The seed maintained constant lunate morphology and hardness, with testa evolving from whitish yellowish to light yellow.



A

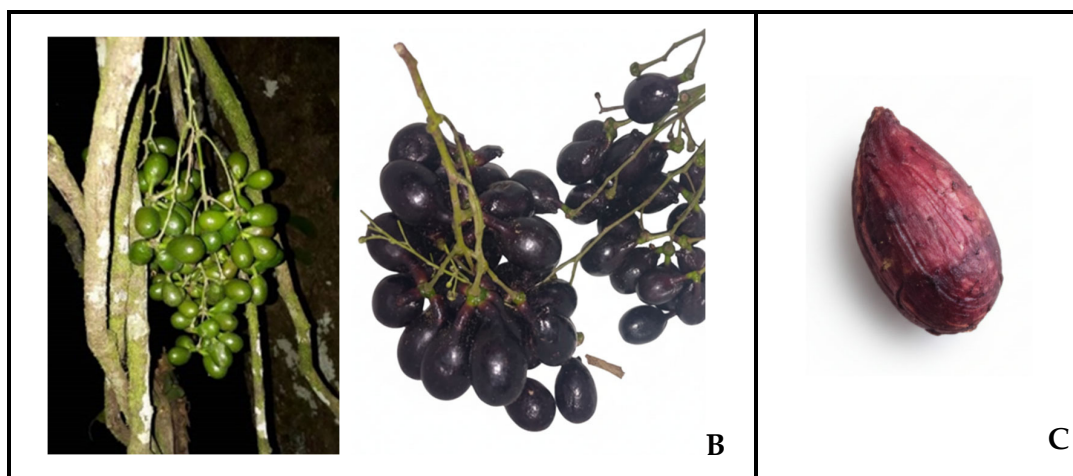





Figure 2. *Mountain grape* morphology. (A) Liana habit showing foliage and flowers. (B) Fruit cluster at physiological and commercial maturity. (C) Lunate seed.

Table 1. Morphological characteristics of *mountain grape* fruits at three maturity stages.

Characteristic	Green (index 0)	Turning (index 1)	Ripe (index 2)
Images			
Shape	Ovoid	Ovoid	Ovoid
Epicarp	Thin, intense green, rough	Thin, yellowish-red, smooth	Thin, blackish-violet, smooth, glossy
Mesocarp	Pale green, firm, darkens upon cutting	Red, semi-fleshy, slightly soft	Garnet, scarce, juicy, soft
Endocarp	Lunate seed, whitish-yellowish testa, hard	Lunate seed, light yellow testa, hard	Lunate seed covered with pulp, light yellow testa, hard

Visual classification by colorimetric index (green = 0, turning = 1, ripe = 2) is used in drupes such as *Olea europaea* and *Prunus spinosa*, where epicarp pigmentation correlates with anthocyanin content, firmness, and physicochemical parameters [14,36]. In *C. tomentosum*, the chromatic transition green → yellowish-red → blackish-violet represents a phenotypic marker of physiological ripening (Table 2).

3.1.2. Biometric Parameters

Fruit dimensions increased progressively during ripening (Table 2). Polar diameter increased from 2.34 ± 0.15 cm (green) to 2.49 ± 0.17 cm (ripe) (+6.4%), while equatorial diameter increased from 1.71 ± 0.15 cm to 1.97 ± 0.14 cm (+15.2%), accompanied by fresh weight gain from 3.89 ± 0.86 g to 5.74 ± 1.07 g (+47.7%; $p < 0.0001$). This growth pattern reflects cell expansion and accumulation of soluble solids characteristic of climacteric ripening in drupes [35,36].

Table 2. Biometric and physicochemical parameters of *mountain grape* fruits at different maturity stages.

Parameter	Green	Turning	Ripe	p-value
Biometric characteristics				

Polar diameter (cm)	2.34 ± 0.15 ^b	2.45 ± 0.22 ^a	2.49 ± 0.17 ^a	<0.0001
Equatorial diameter (cm)	1.71 ± 0.15 ^b	1.90 ± 0.18 ^a	1.97 ± 0.14 ^a	<0.0001
Weight (g)	3.89 ± 0.86 ^b	5.24 ± 1.31 ^a	5.74 ± 1.07 ^a	<0.0001
Physicochemical characteristics				
Vitamin C (mg/100 g fresh sample)	5.12 ± 0.01 ^b	4.78 ± 0.01 ^c	10.22 ± 0.01 ^a	<0.0001
TSS (°Brix)	7.00 ± 0.00 ^c	7.50 ± 0.00 ^b	8.83 ± 0.29 ^a	<0.0001
pH	6.28 ± 0.04 ^a	4.60 ± 0.02 ^b	4.27 ± 0.02 ^c	<0.0001
Titratable acidity (%)	0.25 ± 0.01 ^c	0.62 ± 0.02 ^b	0.94 ± 0.02 ^a	<0.0001
Maturity index	27.82 ± 0.83 ^c	12.13 ± 0.38 ^b	9.42 ± 0.49 ^a	<0.0001

Note. Values expressed as mean ± SD (n = 50). Different superscripts in the same row indicate significant differences (Tukey, $\alpha = 0.05$). TSS: total soluble solids.

Vitamin C content doubled from green to ripe phase (10.22 ± 0.01 vs. 5.12 ± 0.01 mg/100 g FW; +99.6%), in line with activation of ascorbate biosynthesis during late ripening observed in *Vaccinium spp.* and other Andean berries [5,35,37]. TSS increased from 7.00 to 8.83 °Brix (+26.1%), which corresponded to the starch-to-sugar conversion and the building up of soluble carbohydrates [36]. At the same time, pH decreased from 6.28 to 4.27 (−32.0%) and titratable acidity increased from 0.25 to 0.94% (+276%), reflecting organic acid accumulation induced by berry ripening [36,38]. The maturity index (TSS/acidity ratio) decreased from 27.82 to 9.42, illustrating that acidity growth was greater than sugar production, which was contrary to common temperate berries and was in line with ripening fruit of tropical species such as *Rubus* and *Vaccinium* [35,39]. The acidic pH and higher TSS at maturity phase are positive for the stability of anthocyanins whose characteristic flavylum cation predominates below pH 5.0, improving extractability properties and chromatic intensity [36,38]. This biochemical framework indicates that ripe fruits maximize pigment content and technological acceptability for extraction of biologically active compounds.

3.2. Proximate Composition of Ripe Fruits

Ripe fruits presented moisture of $90.45 \pm 0.47\%$, ash of $2.04 \pm 0.14\%$, crude protein of 1.70 ± 0.02 g/100 g, crude fiber of 2.49 ± 0.01 g/100 g, crude fat of 0.05 ± 0.01 g/100 g, and carbohydrates by difference of 3.01 ± 0.49 g/100 g (dry basis). The high water content classifies *C. tomentosum* as an aqueous matrix comparable to grumixama (*Eugenia brasiliensis*, 86.2–89.9%) [40] and superior to cauchao (*Amomyrtus luma*, 75.3%) [37], favoring hydroalcoholic extraction of water-soluble metabolites [41].

The ash fraction exceeded 3.6–6.0 times the values of cauchao (0.57%) [37] and grumixama (0.34–0.49%) [40], suggesting high mineral content associated with montane volcanic soil [42]. Protein content was comparable to cauchao (1.73 g/100 g) [37] but higher than grumixama (0.65–0.83 g/100 g) [40]. The extremely low lipid content (2.3% of cauchao's value) confirms the characteristic profile of pigmented drupes where phenolic metabolites predominate over structural lipids [40,41]. This high-moisture, low-lipid matrix minimizes apolar interferences and maximizes solvent diffusion toward epidermal vacuoles rich in anthocyanins [37,41].

3.3. Ultrasound-Assisted Extraction Optimization

3.3.1. Box-Behnken Experimental Design

The Box-Behnken design evaluated 15 combinations of methanol (25–75%, v/v), ultrasonic amplitude (30–70%), and time (1–15 min) on anthocyanins, total phenols, and antioxidant capacity (Table 3). Response ranges were 42.64–120.82 mg C3G/L, 372.05–677.67 mg GAE/100 g, and 1869.09–5799.38 $\mu\text{mol TE}/100\text{ g}$, respectively, demonstrating variability of 2.8, 1.8, and 3.1-fold between extreme conditions. This second-order factorial design allows modeling linear, quadratic, and interaction effects with a reduced number of experiments compared to full factorial designs [15,16,43].

Table 3. Box-Behnken design and experimental responses for UAE of *mountain grape* in ripe stage.

Methanol (%)	Amplitude (%)	Time (min)	Response variables		
			Anthocyanins ^a	Total phenols ^b	Antioxidant capacity ^c
25 (-1)	30 (-1)	8 (0)	50.50 ± 1.28	431.45 ± 3.74	3106.72 ± 91.39
25 (-1)	50 (0)	1 (-1)	42.64 ± 0.64	372.05 ± 0.79	1869.09 ± 111.22
25 (-1)	50 (0)	15 (+1)	64.87 ± 2.61	608.97 ± 3.70	3784.06 ± 118.17
25 (-1)	70 (+1)	8 (0)	54.02 ± 1.58	525.86 ± 3.94	3491.38 ± 104.96
50 (0)	30 (-1)	1 (-1)	54.45 ± 0.79	386.91 ± 3.34	2688.60 ± 115.43
50 (0)	30 (-1)	15 (+1)	85.34 ± 2.64	576.94 ± 3.80	3758.98 ± 137.04
50 (0)	50 (0)	8 (0)	77.38 ± 0.72	572.04 ± 3.51	3859.33 ± 148.29
50 (0)	50 (0)	8 (0)	71.93 ± 1.68	516.29 ± 2.40	3725.53 ± 142.78
50 (0)	50 (0)	8 (0)	77.96 ± 1.58	535.42 ± 3.97	3625.18 ± 74.98
50 (0)	70 (+1)	1 (-1)	69.63 ± 1.45	441.83 ± 1.00	2872.57 ± 127.04
50 (0)	70 (+1)	15 (+1)	118.58 ± 2.57	677.67 ± 4.12	5799.38 ± 155.35
75 (+1)	30 (-1)	8 (0)	93.41 ± 2.15	538.73 ± 3.24	3449.57 ± 138.29
75 (+1)	50 (0)	1 (-1)	66.53 ± 1.21	448.27 ± 1.46	3098.35 ± 132.38
75 (+1)	50 (0)	15 (+1)	120.82 ± 1.79	667.21 ± 3.13	5581.96 ± 131.48
75 (+1)	70 (+1)	8 (0)	104.36 ± 2.81	547.09 ± 3.32	4469.78 ± 156.46

Note. Response variables expressed as ^a mg cyanidin-3-glucoside/L; ^b mg GAE/100 g; ^c $\mu\text{mol Trolox}/100\text{ g}$.

The quadratic models were statistically significant ($p\text{-model} \leq 0.0037$) with R^2 of 97.62% (anthocyanins), 98.28% (phenols), and 96.57% (antioxidants), confirming robust predictive fit comparable to studies in *Aronia melanocarpa* ($R^2 = 0.99$) [15], *Myrciaria cauliflora* ($R^2 = 0.98$) [16], and *Prunus domestica* ($R^2 = 0.97$) [43]. The absence of residual autocorrelation (Durbin-Watson: 1.16–2.64; $p > 0.05$) validated independence of experimental errors [44,45]. The predictive equations in coded variables were:

$$\text{Anthocyanins} = 75.755 + 21.635A + 7.862B + 19.544C - 8.466A^2 + 8.1B^2 + 4.387C^2 + 1.857AB + 8.016AC + 4.515BC \dots \text{Equation 5}$$

$$\text{Total phenols} = 541.251 + 32.871A + 32.302B + 110.217C - 27.183A^2 - 33.302B^2 - 7.067C^2 - 21.512AB - 4.495AC + 11.454BC \dots \text{Equation 6}$$

$$\text{Antioxidant capacity} = 3736.68 + 543.55A + 453.656B + 1049.47C - 303.831A^2 + 89.198B^2 - 2.787C^2 + 158.884AB + 142.16AC + 464.109BC \dots \text{Equation 7}$$

Linear effects of methanol (A), amplitude (B), and time (C) were significant for all three responses ($p \leq 0.015$), indicating monotonic increase toward upper levels like UAE optimizations in

berries [16,43,44]. Quadratic terms lacked significance ($p \geq 0.17$), suggesting absence of interior optimum and confirming that maximum conditions are located at the boundaries of the experimental space [15,45]. Two interactions were relevant: A×C increased anthocyanins ($p = 0.048$) and B×C increased antioxidant capacity ($p = 0.0319$), demonstrating synergy between solvent-time and amplitude-time respectively, consistent with ultrasonic cavitation mechanisms where prolonged times potentiate methanol and mechanical energy effects on cell disruption [16,44].

3.3.2. ANOVA Fit and Regression Coefficients

The quadratic models were significant ($p \leq 0.0037$) with R^2 of 97.62% (anthocyanins), 98.28% (phenols), and 96.57% (antioxidants), without residual autocorrelation (Durbin-Watson: 1.16–2.64; $p > 0.05$). Regression coefficients (see Table 4) demonstrated the linear effect of methanol (A), amplitude (B), and time (C) on all ($p \leq 0.015$) of the 3 responses, showing the monotonic increase. In summary, the non-significant terms showed no significance in quadratic variables ($p \geq 0.17$), indicative of optimal at experimental space limits consistent with Fernández et al. [16] and Vázquez et al. [15]. The A×C interaction enhanced anthocyanins ($p = 0.048$) and B×C was found to provide the enhanced antioxidant capacity ($p = 0.032$), confirming solvent-time and amplitude-time synergy associated with ultrasonic cavitation mechanisms [43,44].

Table 4. Estimated regression coefficients (β), standard errors (SD), and p-values for quadratic models fitted for bioactive compound extraction and antioxidant capacity.

Term	Anthocyanins (mg Total cyanidin-3-glucoside/L)			phenols (mg Total GAE/100 g)			Antioxidant capacity (uMol Trolox/100 g)		
	β	SD	P-value	β	SD	p-value	β	SD	P-value
Intercept	75.755	–	–	541.251	–	–	3736.68	(–)	–
A (Methanol)	21.635	-2.179	0.0002	32.871	-7.196	0.006	543.55	-111.294	0.0045
B (Amplitude)	7.862	-2.179	0.0154	32.302	-7.196	0.0065	453.656	-111.294	0.0096
C (Time)	19.544	-2.179	0.0003	110.217	-7.196	<0.0001	1049.47	-111.294	0.0002
A²	-8.466	-6.415	0.2442	-27.183	-21.184	0.2557	-303.831	-327.641	0.3963
B²	8.1	-6.415	0.2624	-33.761	-21.184	0.1719	89.198	-327.641	0.7963
C²	4.387	-6.415	0.5245	-7.067	-21.184	0.7522	-2.787	-327.641	0.9935
AB	1.857	-3.082	0.5731	-21.512	-10.176	0.0882	158.884	-157.394	0.3591
AC	8.016	-3.082	0.0482	-4.495	-10.176	0.6771	142.16	-157.394	0.4078
BC	4.515	-3.082	0.2028	11.454	-10.176	0.3115	464.109	-157.394	0.0319

Note. A: methanol concentration (% v/v), B: sonication amplitude (%), C: extraction time (min). Bold p-values < 0.05.

3.3.3. Response Surfaces and Mechanistic Interpretation

The 3D response surfaces (Figures 3–6) illustrate the combined effects of methanol and amplitude at fixed time of 15 min on the three responses. The anthocyanin surface (Figure 3) shows progressive increase from 60 mg C3G/L (25% methanol, 30% amplitude) to 151 mg C3G/L (75% methanol, 70% amplitude), with color gradient transitioning from blue (low values) to red (high values). The elongated diagonal contours toward the upper right corner indicate synergistic effect between solvent concentration and ultrasonic energy. This pattern confirms that elevated methanol concentrations improve solubilization of glycosylated anthocyanins by reducing medium polarity,

while higher amplitudes intensify acoustic cavitation that disrupts epidermal vacuoles rich in pigments [16,43].

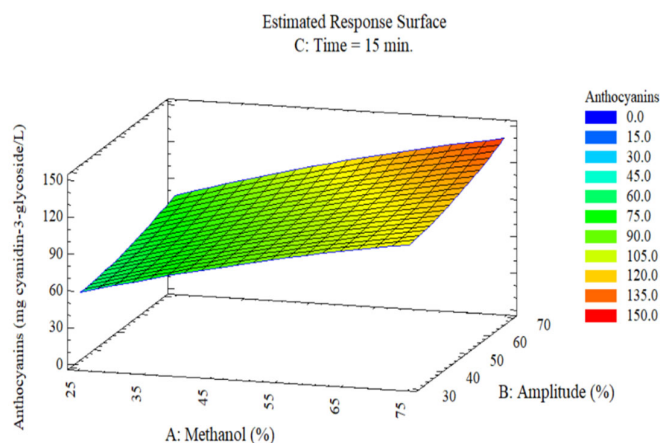


Figure 3. Response surface of the effect of methanol (A) and ultrasonic amplitude (B) on (C) anthocyanin content in *C. tomentosum* fruits (time = 15 min).

The antioxidant capacity surface (Figure 4) exhibits analogous behavior, increasing from 3200 $\mu\text{mol TE}/100\text{ g}$ (minimum conditions) to 6200 $\mu\text{mol TE}/100\text{ g}$ (maximum conditions), representing a 2.0-fold increase. The surface shows parallel contours without pronounced interior curvature, consistent with the absence of significant quadratic terms (Table 4; $p \geq 0.17$) and confirming additive effects of methanol and amplitude. The linear increase reflects that reducing capacity measured by DPPH increases proportionally with the extraction of total phenolic compounds and anthocyanins, main contributors to antioxidant activity [15,44].

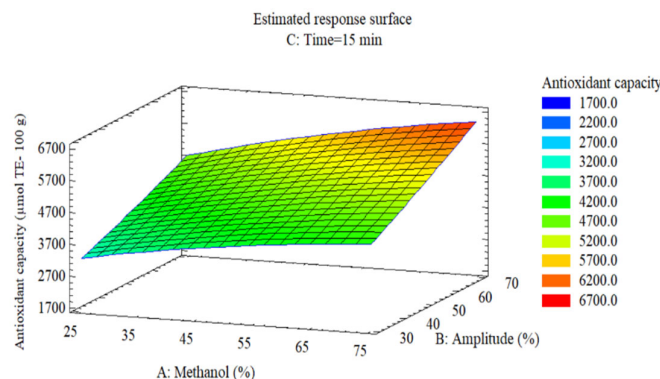


Figure 4. Response surface of the effect of methanol (A) and ultrasonic amplitude (B) on (C) antioxidant capacity ($\mu\text{mol Trolox}/100\text{ g}$) at 15 min.

Total phenols (Figure 5) present a surface with increase from 500 mg GAE/100 g to 670 mg GAE/100 g, showing greater influence of methanol (coefficient $\beta = 32.87$; $p = 0.006$) than amplitude ($\beta = 32.30$; $p = 0.007$). The more widely spaced contours in the direction of the methanol axis evidence its dominant effect on phenolic recovery. The optimal region is located at the upper boundary of the experimental space ($\geq 65\%$ methanol, $\geq 60\%$ amplitude), confirming absence of interior maximum. Mechanistically, methanol facilitates rupture of ester bonds between phenolics and cell wall

polysaccharides, while ultrasound accelerates mass transfer by localized microagitation in bubble collapse zones of cavitation [43,45].

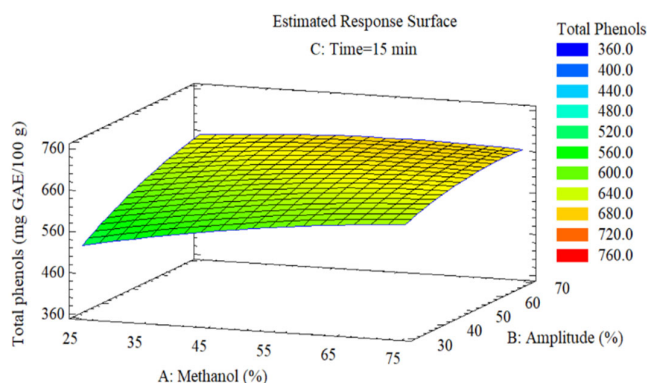


Figure 5. Response surface of the effect of (A) methanol and (B) ultrasonic amplitude on (C) total phenol content (mg GAE/100 g) at 15 min.

3.3.4. Multi-Response Optimization and Validation

The desirability surface (Figure 6) identifies the optimal region at 57% methanol, 70% amplitude, and 15 min (desirability = 0.9996), represented by the red zone in the upper right corner where the three optimal responses converge. Desirability transitions from 0.4 (blue, minimum conditions) to 1.0 (red, optimal conditions), demonstrating simultaneous maximization without trade-offs between objectives. Experimental validation (Table 5) confirms 120.71 ± 1.89 mg C3G/L, 672.46 ± 5.84 mg GAE/100 g, and 5857.31 ± 60.20 $\mu\text{mol TE}/100$ g, with deviations of 1.69%, 0.47%, and 2.07% from predicted values, within acceptable limits (< 5%) for RSM models [44].

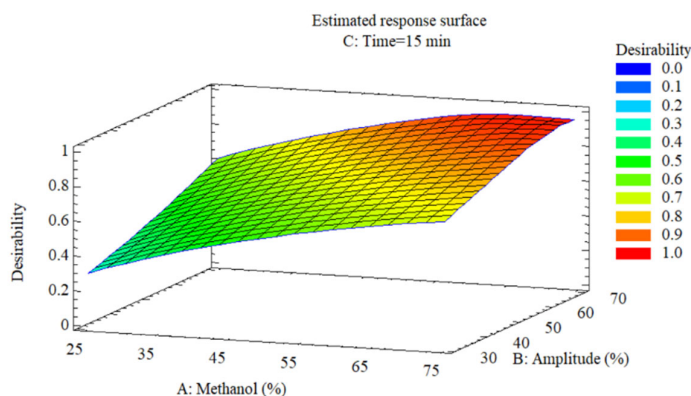


Figure 6. Multi-response optimization through desirability function: optimal operating region for simultaneous maximization of anthocyanins, total phenols, and antioxidant capacity.

Table 5. Experimental validation of the optimal point (57% MeOH, 70% amplitude, 15 min).

Response	Perdition	Experimental	Error (%)
Anthocyanins (mg C3G/L)	122.79	120.71 ± 1.89	1.69
Total Phenols (mg GAE/100 g)	675.65	672.46 ± 5.84	0.47
Antioxidants ($\mu\text{mol TE}/100$ g)	5981	5857.31 ± 60.20	2.07

3.4. Application of Optimal Conditions Across Maturity Stages

Under optimized UAE conditions (57% methanol, 70% amplitude, 15 min), maturity stage determined significant differences in all three responses (ANOVA, $p < 0.0001$; Table 6). Monomeric anthocyanins were undetectable in green fruits, reached 46.01 ± 0.70 mg C3G/L in turning fruits, and 120.71 ± 1.89 mg C3G/L in ripe fruits (+162% vs. turning; $p < 0.0001$). This progressive increase reflects activation of the phenylpropanoid biosynthetic pathway during ripening, responsible for anthocyanin synthesis through sequential action of chalcone synthase, flavanone 3-hydroxylase, and UDP-glucose:flavonoid 3-O-glucosyltransferase [34,35,38]. Additionally, cell wall softening mediated by pectinases and cellulases in ripe stages facilitates mechanical disruption by ultrasonic cavitation, increasing release of vacuolar anthocyanins [14,16].

Table 6. Bioactive compounds extracted under optimal UAE conditions (57% MeOH, 70% amplitude, 15 min) at three maturity stages of *mountain grape*.

Maturity stage	Anthocyanins (mg C3G/L)*	Total phenols (mg GAE/100 g)**	Antioxidant capacity ($\mu\text{mol TE}/100 \text{ g}$)***
Green (0)	0.00 ± 0.00 c	647.83 ± 3.55 b	5492.63 ± 54.30 b
Turning (3)	46.01 ± 0.70 b	458.86 ± 5.66 c	3581.11 ± 39.80 c
Ripe (7)	120.71 ± 1.89 a	672.46 ± 5.84 a	5857.55 ± 60.20 a

Note. Values represent mean \pm SD ($n = 3$). Different letters in the same column indicate significant differences (Tukey, $\alpha = 0.05$). *Expressed as cyanidin-3-glucoside equivalents; **expressed as gallic acid equivalents on fresh weight basis; ***expressed as Trolox equivalents on fresh weight basis.

Total phenols exhibited a nonlinear pattern during ripening. The turning stage registered the minimum value (458.86 ± 5.66 mg GAE/100 g), while ripe reached the maximum (672.46 ± 5.84 mg GAE/100 g; +46.7% vs. turning; $p < 0.0001$), slightly exceeding green (647.83 ± 3.55 mg GAE/100 g; +3.8% vs. green). The transient depression in turning coincides with the rapid cell expansion phase, where dilution by water accumulation and metabolic reconfiguration toward anthocyanin biosynthesis temporarily reduce the total phenolic pool [5,34,35]. In contrast, the ripe stage combines net accumulation of structural phenols (hydroxycinnamic acids) with newly synthesized anthocyanins, resulting in maximum phenolic content [38,41].

Antioxidant capacity followed a trend analogous to total phenols: turning < green < ripe ($3581.11 \pm 39.80 < 5492.63 \pm 54.30 < 5857.55 \pm 60.20$ $\mu\text{mol TE}/100 \text{ g}$). The +63.6% increase between turning and ripe ($p < 0.0001$) correlates with synchronized accumulation of anthocyanins (+162%) and total phenols (+46.7%), evidencing additive contribution of both metabolite families to reducing activity measured by DPPH [15,34]. The acidic pH of the ripe stage (4.27 ± 0.02 ; Table 1) additionally favors stability of the flavylium cation (predominant form of anthocyanins at $\text{pH} < 5$), maximizing its antioxidant activity through electronic resonance of the oxonium ring [36,38].

3.5. Principal Component Analysis

PCA on eight physicochemical and bioactive variables explained 90.6% of total variability (PC1 = 67.4%, PC2 = 23.2%; Figure 7). PC1 ordered samples according to ontogenic gradient: green fruits in negative PC1, ripe in positive PC1, turning in intermediate positions. This separation reflects metabolic transition during ripening [5,35].

TSS, vitamin C, anthocyanins, total phenols, antioxidant capacity, and acidity presented positive loadings on PC1, associated with ripe fruits. pH and maturity index showed negative loadings, associated with green fruits. This configuration agrees with Table 1 data: TSS increased +26.1% (7.00 \rightarrow 8.83 $^\circ\text{Brix}$), vitamin C +99.6%, acidity +276% (0.25 \rightarrow 0.94%), while pH decreased 32.0% (6.28 \rightarrow 4.27) and maturity index -66.1% (27.82 \rightarrow 9.42). This pattern, where acidity exceeds sugar

accumulation, is characteristic of Andean and tropical berries of *Vaccinium* and *Rubus*, differing from temperate fruits [34,39,41].

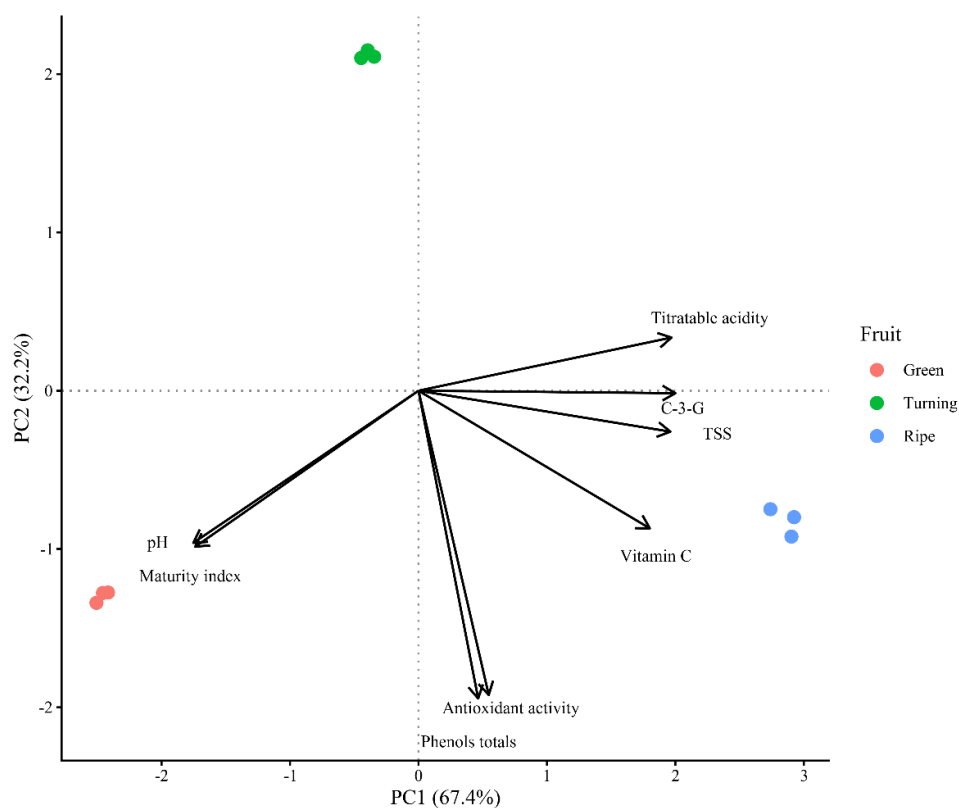


Figure 7. Principal component analysis biplot of physicochemical and bioactive variables in *mountain grape* fruits according to maturity stage. PC1 explains 67.4% and PC2 explains 23.2% of total variability.

PC2 differentiated the turning stage, which projected separately from green and ripe. This separation captures the transient metabolic minimum in turning: total phenols (458.86 mg GAE/100 g; -29.2% vs. green) and antioxidant capacity (3581.11 $\mu\text{mol TE}/100\text{ g}$; -34.8% vs. green; Table 5). This valley coincides with rapid cell expansion, where water dilution and biosynthetic reorientation toward anthocyanins temporarily reduce the extractable phenolic pool [5,35]. *Vaccinium corymbosum* and *Rubus ulmifolius* exhibit analogous minima at intermediate stages [34,38].

The standardized z-score heatmap confirmed differentiation by maturity (Figure 8). Ripe fruits presented positive z-scores in anthocyanins, total phenols, antioxidant capacity, vitamin C, TSS, and **acidity**, negative in pH and maturity index. This pattern indicates co-accumulation of primary (sugars, ascorbate) and secondary (phenols, anthocyanins) metabolites, characteristic of pigmented berries where ripening integrates shikimate, phenylpropanoid, and ascorbate-glutathione pathways [38,41]. Turning showed minimum z-scores exclusively in phenols and antioxidant capacity, confirming its metabolic transition.

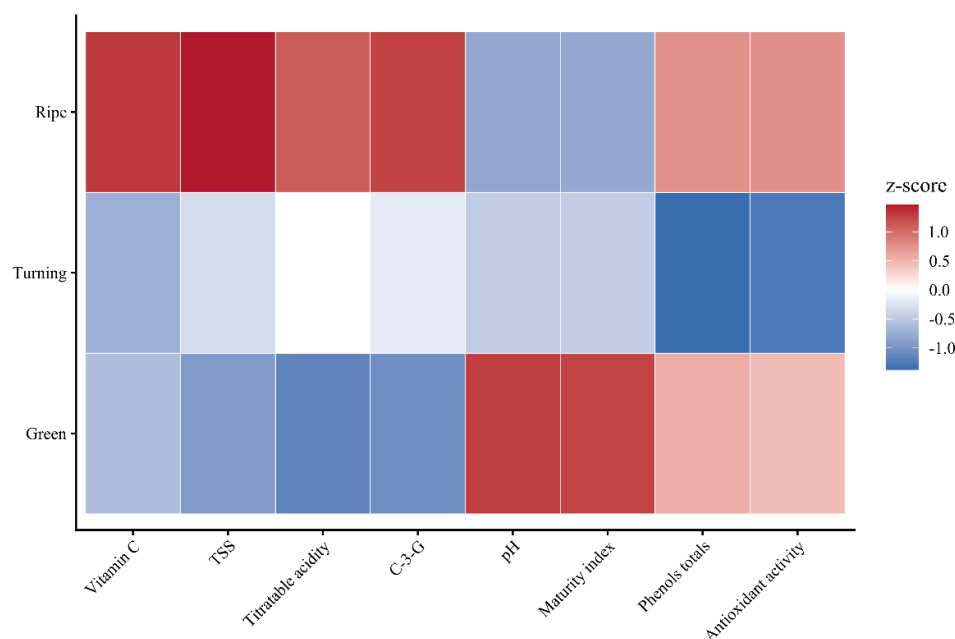


Figure 8. Heatmap of z-scores of physicochemical and bioactive variables at three maturity stages of *mountain grape*. Red: values above mean ($z > 0$); blue: values below mean ($z < 0$).

Vacuolar acidification in ripe fruits (pH 4.27; Table 1) optimizes bioactive compounds under UAE. Acidic pH stabilizes the flavylium cation (predominant form at $\text{pH} < 5$), preventing conversion to colorless forms and maximizing chromophoric content and antioxidant activity [36,38]. Furthermore, the acidic environment protonates phenolic hydroxyl groups in hydroalcoholic mixtures allowing greater solubility in them and also in optimizing UAE efficiency [14,16]. This association between ripening physiology and extraction method enables ripe fruit to maximise all three responses at the same time (Table 5): 120.71 mg C3G/L (+162% vs. turning), 672.46 mg GAE/100 g (+46.7% vs. turning), 5857.55 $\mu\text{mol TE}/100 \text{ g}$ (+63.6% vs. turning).

The findings demonstrate that *C. tomentosum* ripening has a progressive bioactive compound accumulation model, which was promoted via vacuolar acidification with a transient metabolic valley in turning. This pattern, along with favorable UAE conditions (57% methanol, 70% amplitude, 15 min) turns ripe fruit into raw materials for natural colorants, nutraceuticals and functional foods from Amazonian berries.

4. Conclusions

Box-Behnken optimization established UAE conditions (57% methanol, 70% amplitude, 15 min) that maximized anthocyanin yield (120.71 mg C3G/L), total phenols (672.46 mg GAE/100 g), and antioxidant capacity (5857.55 $\mu\text{mol TE}/100 \text{ g}$) from ripe *C. tomentosum* fruits with high predictive accuracy ($R^2 > 0.95$, 2.1% deviation). Ripening from green to ripe stage triggered a 162% increase in anthocyanins and 46.7% increase in total phenols, driven by vacuolar acidification (pH 4.27) that stabilizes anthocyanin structure and enhances UAE extractability. The transitory metabolic valley at turning stage (-29.2% phenols, -34.8% antioxidant capacity) reflects biosynthetic reorganization during cell expansion, establishing an ontogenic pattern where acidification predominates over sugar accumulation. Proximate composition (90.45% moisture, 2.04% ash, 2.49% fiber, 1.70% protein) positions *C. tomentosum* as a hydrophilic matrix comparable to Andean berries, favoring hydroalcoholic extraction of water-soluble bioactives. These findings establish ripe *C. tomentosum* fruits as a promising raw material for natural colorants and functional food ingredients derived from underexploited Amazonian biodiversity.

Author Contributions: D.H-H.: conceptualization, investigation, formal analysis, writing—original draft preparation, writing—review and editing. H.M.-V.: formal analysis, writing—original draft preparation, writing—review, and editing. S.C-Q.: formal analysis, writing—original draft preparation, writing—review, and editing. L.M-C.: writing—review, and editing, validation and visualization. R.R-B.: writing—review and editing, and supervision. All authors have read and agreed to the published version of the manuscript.

Funding: This research was funded by PROINTEC-2023 (Proyectos de Investigación, Innovación y Desarrollo Tecnológico) under agreement No. 05-2023-UNJ/PCO with the Universidad Nacional de Jaén.

Data Availability Statement: Data are contained within the article.

Acknowledgments: This research was conducted with institutional support from the Universidad Nacional del Santa (UNS). The authors would also like to thank PROINTEC-2023 for its funding and Elver Peralta, a farmer, for facilitating our access to the fruits of *Chondrodendron tomentosum* (mountain grapes).

Conflicts of Interest: The authors declare no potential financial or other interests that could be perceived to influence the outcomes of this research. No conflict, informed consent, human or animal rights applicable.

Abbreviations

ANOVA	Analysis of variance
AOAC	Association of Official Analytical Chemists
BBD	Box-Behnken design
C3G	Cyanidin-3-glucoside
DPPH	2,2-diphenyl-1-picrylhydrazyl
FRAP	Ferric reducing antioxidant power
GAE	Gallic acid equivalents
MI	Maturity index
RSM	Response surface methodology
TA	Titrateable acidity
TAC	Total anthocyanin content
TE	Trolox equivalents
TPC	Total phenolic content
TSS	Total soluble solids
UAE	Ultrasound-assisted extraction

References

1. Cañigual, S. Plantas Medicinales y Drogas Vegetales. *OFFARM* **2003**, *22*, 161–162.
2. Chondrodendron Tomentosum Available online: <https://ntbg.org/database/plants/detail/chondrodendron-tomentosum> (accessed on 13 October 2025).
3. Instituto de Salud Pública Curare, Pareira. **2021**, 9–11.
4. Atongbiik, M.; Olaide, R.; Hensel, O.; Sturm, B.; Kudadam, J. Nutritional Characteristics of Four Underutilized Edible Wild Fruits of Dietary Interest in Ghana. *Foods* **2019**, *8*, 1–12, doi:<https://doi.org/10.3390/foods8030104>.
5. Ayuso, M.; Cruz, F.; Ramos, M.; Nicolás, N.; Ramos, M.; Rodríguez, M.; Calvo, P. Characterization and Classification of Berry (Aronia, Haskap, and Goji) Fruits with High Bioactive Value Grown in Spain. *Foods* **2024**, *13*, 1–15, doi:<https://doi.org/10.3390/foods13244122>.
6. Feng, C.; Su, S.; Wang, L.; Wu, J.; Tang, Z.; Xu, Y.; Shu, Q.; Wang, L. Antioxidant Capacities and Anthocyanin Characteristics of the Black–Red Wild Berries Obtained in Northeast China. *Food Chem.* **2016**, *204*, 150–158, doi:<https://doi.org/10.1016/j.foodchem.2016.02.122>.
7. Vega, A.; Rodríguez, Á.; Stucken, K. Antioxidant, Functional Properties and Health-promoting Potential of Native South American Berries: A Review. *J. Sci. Food Agric.* **2021**, *101*, 364–378, doi:<https://doi.org/10.1002/jsfa.10621>.
8. Bozdogan, N.; Yıldız, E.; Tunç, Y.; Khadivi, A.; Yaman, M.; Sümbül, A.; Ugurtan, K.; Ates, U.; Oztürk, B. Morphological, Biochemical, and Molecular Characterizations of Rosehip (*Rosa Canina* L.) Genotypes

- Naturally Grown in the Eastern Central Anatolia Region of Türkiye. *Sci. Hortic. (Amsterdam)*. **2025**, *350*, 114375, doi:https://doi.org/10.1016/j.scienta.2025.114375.
9. Ercisli, S.; Ibrahim, H. Wild Edible Fruits: A Rich Source of Biodiversity. *ANADOLU Ege Tarımsal Araştırma Enstitüsü Derg.* **2017**, *27*, 116–122.
 10. Bhadange, Y.; Carpenter, J.; Kumar, V. A Comprehensive Review on Advanced Extraction Techniques for Retrieving Bioactive Components from Natural Sources. *ACS Omega* **2024**, *9*, 31274–31297, doi:https://doi.org/10.1021/acsomega.4c02718.
 11. Carpentieri, S.; Soltanipour, F.; Ferrari, G.; Pataro, G.; Donsi, F. Emerging Green Techniques for the Extraction of Antioxidants from Agri-Food by-Products as Promising Ingredients for the Food Industry. *Antioxidants* **2021**, *10*, 1417, doi:https://doi.org/10.3390/antiox10091417.
 12. Athanasiadis, V.; Chatzimitakos, T.; Mantiniotou, M.; Kalompatsios, D.; Kotsou, K.; Makrygiannis, I.; Bozinou, E.; Lalas, S. Optimization of Four Different Rosemary Extraction Techniques Using Plackett–Burman Design and Comparison of Their Antioxidant Compounds. *Int. J. Mol. Sci.* **2024**, *25*, 7708, doi:https://doi.org/10.3390/ijms25147708.
 13. Hong, C.; Ching, M.; Pin, S.; Ling, N. A Review on Extraction Techniques and Its Future Applications in Industry. *Eur. J. Lipid Sci. Technol.* **2021**, *123*, 1–10, doi:https://doi.org/10.1002/ejlt.202000302.
 14. González, A.; Vázquez, M.; Espada, E.; Ferreira, M.; Carrera, C.; Palma, M.; Álvarez, J.; Barbero, G.; Ayuso, J. Optimization of Analytical Ultrasound-Assisted Methods for the Extraction of Total Phenolic Compounds and Anthocyanins from Sloes (*Prunus Spinosa* L.). *Agronomy* **2020**, *10*, 1–22, doi:https://doi.org/10.3390/agronomy10070966.
 15. Vázquez, M.; González, A.; Espada, E.; Ferreira, M.; Toledo, J.; Carrera, C.; Palma, M.; Barbero, G. Ultrasound-Assisted Extraction of Two Types of Antioxidant Compounds (TPC and TA) from Black Chokeberry (*Aronia Melanocarpa* L.): Optimization of the Individual and Simultaneous Extraction Methods. *Agronomy* **2019**, *9*, 456, doi:https://doi.org/10.3390/agronomy9080456.
 16. Fernández, G.; Pinedo, C.; Espada, E.; Ferreira, M.; Carrera, C.; Palma, M.; García, C. Optimization of Ultrasound-Assisted Extraction of Bioactive Compounds from Jabuticaba (*Myrciaria Cauliflora*) Fruit through a Box-Behnken Experimental Design. *Food Sci. Technol.* **2019**, *39*, 1018–1029, doi:https://doi.org/10.1590/fst.16918.
 17. González, A.; Vázquez, M.; Espada, E.; Ferreira, M.; Amores, A.; Palma, M.; Barbero, G.; Jiménez, A. Alternative Ultrasound-Assisted Method for the Extraction of the Bioactive Compounds Present in Myrtle (*Myrtus Communis* L.). *Molecules* **2019**, *24*, 882, doi:https://doi.org/10.3390/molecules24050882.
 18. Espada, E.; Ferreira, M.; Carrera, C.; Palma, M.; Barroso, C.; Barbero, G. Optimization of the Ultrasound-Assisted Extraction of Anthocyanins and Total Phenolic Compounds in Mulberry (*Morus Nigra*) Pulp. *Food Chem.* **2017**, *219*, 23–32, doi:https://doi.org/10.1016/j.foodchem.2016.09.122.
 19. Justicia, M.; Madueño, A.; Ruiz, A.; Molina, J.; López, M.; Madueño, J.; Granados, J. Low-Frequency Characterisation of Mesocarp Electrical Conductivity in Different Varieties of Olives (*Olea Europaea* L.). *Comput. Electron. Agric.* **2017**, *142*, 338–347, doi:https://doi.org/10.1016/j.compag.2017.09.021.
 20. Safy, S.; Khalifa, A.; Almashad, A.; Mohamed, A.; Hammad, E.; Sami, R.; Aljahani, A.; Pareek, S.; Helal, M.; Alharthi, S.; et al. Utilization of Jamun Fruit (*Syzygium Cumini* L.) for Value Added Food Products. *J. Food Qual.* **2023**, 5460642, doi:https://doi.org/10.1155/2023/5460642.
 21. McCullum, R.; Saifullah, M.; Bowyer, M.; Vuong, Q. Characteristics, Bioactives and Antioxidant Activity of Illawarra Plum (*Podocarpus Elatus*) Fruit. *eFood* **2025**, *6*, e70088, doi:https://doi.org/10.1002/efd2.70088.
 22. Rymbai, H.; Kumar, J.M.V.; Kumar, S.; Hazarika, S.; Ercisli, S.; Kumar, V.; Sulusoglu, M. Maturity Stages Modulate Fruit Quality, Bioactive Constituents, and Antioxidant Activity of *Prunus Jenkinsii*. *Genet. Resour. Crop Evol.* **2023**, *71*, 1541–1555, doi:https://doi.org/10.1007/s10722-023-01718-1.
 23. AOAC INTERNATIONAL Official Method 967.21: Vitamin C. In: Official Methods of Analysis of AOAC INTERNATIONAL, 2019; pp. 21–22.
 24. Latimer, G.W. *Official Methods of Analysis of AOAC INTERNATIONAL*; 22nd ed.; Oxford University Press, 2023; ISBN https://doi.org/10.1093/9780197610145.001.0001.
 25. Santos, J.; Damiani, C.; Crivelari, M.; Nunes, E.; Vilas, E. Volatile Profiling of Pitanga Fruit (*Eugenia Uniflora* L.) at Different Ripening Stages Using Solid-Phase Microextraction and Mass Spectrometry

- Coupled with Gas Chromatography. *Sci. Hortic. (Amsterdam)*. **2019**, *250*, 366–370, doi:https://doi.org/10.1016/j.scienta.2019.02.076.
26. AOAC INTERNATIONAL Official Method 954.01: Crude Protein. In; Official Methods of Analysis of AOAC INTERNATIONAL, 2019; p. 24.
 27. NTP Peruvian Technical Standard 205.003: Cereals and Legumes. Determination of Crude Fiber. In; National Quality Institute, 2011; pp. 1–5.
 28. AOAC INTERNATIONAL Official Method 930.09: Fat. In; Official Methods of Analysis of AOAC INTERNATIONAL, 2019; p. 24.
 29. Christou, A.; Stavrou, I.; Kapnissi, C. Continuous and Pulsed Ultrasound-Assisted Extraction of Carob's Antioxidants: Processing Parameters Optimization and Identification of Polyphenolic Composition. *Ultrason. Sonochem.* **2021**, *76*, 105630, doi:https://doi.org/10.1016/j.ultsonch.2021.105630.
 30. Razola, M.; Aznar, M.; Guerra, E.; García, B.; Gómez, A.; Verardo, V. Establishment of a Sonotrode Ultrasound-Assisted Extraction of Phenolic Compounds from Apple Pomace. *Foods* **2022**, *11*, 3809, doi:https://doi.org/10.3390/foods11233809.
 31. Alvarez, E.; de la Rosa, L.; Amarowicz, R.; Shahidi, F. Antioxidant Activity of Fresh and Processed Jalapeño and Serrano Peppers. *J. Agric. Food Chem.* **2011**, *59*, 163–173, doi:10.1021/jf103434u.
 32. Lee, J.; Durst, R.; Wrolstad, R. Determination of Total Monomeric Anthocyanin Pigment Content of Fruit Juices, Beverages, Natural Colorants, and Wines by the PH Differential Method: Collaborative Study. *J. AOAC Int.* **2005**, *88*, 1269–1278, doi:https://doi.org/10.1093/jaoac/88.5.1269.
 33. Pырzыnska, K.; Pekal, A. Application of Free Radical Diphenylpicrylhydrazyl (DPPH) to Estimate the Antioxidant Capacity of Food Samples. *Anal. Methods* **2013**, *5*, 4288–4295, doi:DOI https://doi.org/10.1039/C3AY40367J.
 34. Castro, R.; Vásquez, C.; Gil, M.; Parra, C.; Ramos, P.; Morales, L. Evolution of the Volatile Organic Compounds, Phenols and Antioxidant Capacity during Fruit Ripening and Development of *Rubus Ulmifolius* Schott Fruits. *Horticulturae* **2022**, *9*, 1–13, doi:https://doi.org/10.3390/horticulturae9010013.
 35. Murcia, A.; Ruiz, H.; Balaguera, H. Estudio Del Crecimiento y Desarrollo Del Fruto de Agraz (*Vaccinium Meridionale* Swartz) Bajo Condiciones de Clima Frío. *Biotechnol. en el Sect. Agropecu. y Agroindustrial* **2021**, *19*, 135–146, doi:https://doi.org/10.18684/bsaa.v19.n2.2021.1613.
 36. Ivancic, T.; Jakopic, J.; Veberic, R.; Vesel, V.; Hudina, M. Effect of Ripening on the Phenolic and Sugar Contents in the Meso- and Epicarp of Olive Fruits (*Olea Europaea* L.) Cultivar 'Leccino.' *Agriculture* **2022**, *12*, 1–17, doi:https://doi.org/10.3390/agriculture12091347.
 37. Gomez, L.; Poblete, J.; García, V.; Vidal, R. Cauchao Berry (*Amomyrtus Luma*) as a Promising Source of Bioactive Compounds: Optimized Extraction, Phytochemical Characterization, and Assessment of Antioxidant and Antidiabetic Potential. *Int. J. Mol. Sci.* **2025**, *26*, 8391, doi:https://doi.org/10.3390/ijms26178391.
 38. Bernal, J.; Molina, J.; Angoa, M.; Cárdenas, J.; García, I.; Ceja, J.; Mena, H. Phenolic Compound Content and the Antioxidant and Antimicrobial Activity of Wild Blueberries (*Vaccinium Stenophyllum* Steud.) Fruits Extracts during Ripening. *Horticulturae* **2022**, *8*, 1–17, doi:https://doi.org/10.3390/horticulturae8010015.
 39. Agostino, M.; Sicari, V.; Giuffrè, A.; Soria, A. Blackberries (*Rubus Ulmifolius* Schott) from Calabria (Italy): A Comprehensive Characterisation. *Eur. Food Res. Technol.* **2022**, *248*, 905–916, doi:https://doi.org/10.1007/s00217-021-03922-8.
 40. Nehring, P.; Tischer, S.; Schulz, M.; Betta, F.; Gonzaga, L.; Vitali, L.; da Silva, M.; Amadeu, G.; Oliveira, A.; Fett, R. Grumixama (*Eugenia Brasiliensis* Lamarck) Functional Phytochemicals: Effect of Environmental Conditions and Ripening Process. *Food Res. Int.* **2022**, *157*, 111460, doi:https://doi.org/10.1016/j.foodres.2022.111460.
 41. Flor, O.; Guanochanga, F.; Samaniego, I.; Arias, V.; Ortiz, B.; Rosales, C.; Palacios, H. Physicochemical Characterization and Antioxidant Capacity of Açai (*Euterpe Oleracea*) in Ecuadorian Region. *Foods* **2024**, *13*, 1–20, doi:https://doi.org/10.3390/foods13193046.
 42. Sasikumar, R.; Kambhampati, V.; Kumar, J.; Paras, S.; Govindasam, K.; Jaiswal, A. Nutritional, Phytochemical, and Toxicological Profiles of Blood Fruit (*Haematocarpus Validus*). *J. Agric. Food Res.* **2025**, *19*, 101731, doi:https://doi.org/10.1016/j.jafr.2025.101731.

43. Drăghici, A.; Părvulescu, O.; Stan, R.; Brezoiu, A. Optimization of Ultrasound-Assisted Extraction of Phenolic Compounds from Romanian Blackthorn (*Prunus Spinosa* L.) Fruits. *Antioxidants* **2025**, *14*, 1–19, doi:<https://doi.org/10.3390/antiox14060680>.
44. Kashyap, P.; Singh, C.; Jindal, N. Polyphenol Bio-Accessibility and Antioxidant Activity of in Vitro Digested Ultrasound-Assisted Meghalayan Cherry (*Prunus Nepalensis*) Pomace Extract. *Biomass Convers. Biorefinery* **2022**, *13*, 14071–14085, doi:<https://doi.org/10.1007/s13399-021-02150-0>.
45. Sousa, L.; Alves, E.; Narciso, F.; Sousa, E.; Silva, I. Optimization of Pressurized Liquid Extraction and Ultrasound Methods for Recovery of Anthocyanins Present in Jambolan Fruit (*Syzygium Cumini* L.). *Food Bioprod. Process.* **2021**, *127*, 77–89, doi:<https://doi.org/10.1016/j.fbp.2021.02.012>.

Disclaimer/Publisher's Note: The statements, opinions and data contained in all publications are solely those of the individual author(s) and contributor(s) and not of MDPI and/or the editor(s). MDPI and/or the editor(s) disclaim responsibility for any injury to people or property resulting from any ideas, methods, instructions or products referred to in the content.